ACS OMEGA

Article

Cite This: ACS Omega 2018, 3, 11117−11127

http://pubs.acs.org/journal/acsodf

Zirconium Modification Promotes Catalytic Activity of a Single-Site Cobalt Heterogeneous Catalyst for Propane Dehydrogenation

Yiqing Zhao,[†,‡] Hyuntae Sohn,[‡,∥] Bo Hu,[†,‡,⊥] Jens Niklas,[‡] Oleg G. Poluektov,[‡] Jun Tian,[§] Massimiliano Delferro,[‡] and Adam S. Hock*[,†,‡]

[†]Department of Chemistry, Illinois Institute of Technology, Chicago, Illinois 60616, United States

[‡]Chemical Sciences and Engineering Division and [§]Center for Nanoscale Materials, Argonne National Laboratory, Lemont, Illinois 60439, United States

Supporting Information

ABSTRACT: The effect of Zr modification on the catalytic activity of Co/SiO_2 was investigated for nonoxidative propane dehydrogenation. Isolated Zr on SiO_2 surface sites were prepared by organometallic synthesis using $Zr(O^tBu)_4$ as a precursor. The resulting Zr/SiO_2 support was functionalized with Co^{2+} ions via strong electrostatic adsorption. Spectroscopic (diffuse reflectance infrared Fourier transform spectroscopy, UV−vis, electron paramagnetic resonance) and microscopic characterization (transmission electron microscopy, scanning transition electron microscopy) results are consistent with single-site cobalt that preferentially associates with the mono-dispersed Zr at a variety of loadings and Co/Zr ratios. The oxidation state of Co in the as-prepared Co/SiO_2 and $Co-Zr/SiO_2$ was both +2 with tetrahedral and octahedral geometries, respectively. In situ X-ray absorption near edge structure and extended X-ray absorption fine structure results confirmed that the oxidation state of Co remained as +2 under reaction condition for both Co/SiO_2 and $Co-Zr/SiO_2$ samples and both catalysts have tetrahedral Co^{2+} as the active catalyst. Despite similar Co coordination environments, the catalytic activity and selectivity was significantly improved by the Zr modification of the silica support versus Co/SiO_2. This was attributed to the change in oxygen donor ability and Co−O bond strength of the ≡SiO−Zr−O sites of $Co-Zr/SiO_2$ compared with the ≡SiO− ligands in Co/SiO_2. These results show that tuning of the support SiO_2 oxygen donation ability by use of an anchoring site (e.g., ≡SiO−Zr−O^-) can be used to alter both rate and selectivity of propane dehydrogenation with single-site heterogeneous catalysts. These results also show some preference for Co^{2+} active sites to associate with ≡SiO−Zr−O^- sites over ≡SiO−.

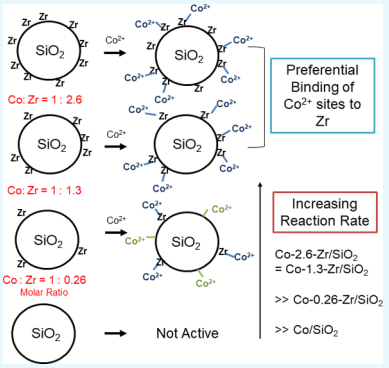

1. INTRODUCTION

On-purpose production of propylene via nonoxidative propane dehydrogenation[1] (PDH) from conventional and shale gas streams is of increasing importance for the olefin and chemical industries. For this process, Pt−Sn and CrO_x supported on alumina and silica catalysts are commercially available today.[2−5] These catalysts have been extensively researched in the literature and the factors that affect their rate and selectivity are well-studied, even if the precise method of modification remains unclear. For example, Bariås et al. studied Pt and Pt−Sn catalytic systems on two different supports Al_2O_3 and SiO_2 for PDH. It was found that on both supports addition of Sn promoted the catalytic activity and stability.[2] Pt−Sn alloys are believed to be superior to pure Pt because of the Sn increasing Pt dispersion, decreasing propene binding energies (decreasing deep dehydrogenation and coking), and breaking up ensembles of Pt atoms that readily cleave C−C bonds.[1−3,6] As might be expected, the support appears to play less of a role in metallic-phase dehydrogenation catalysts than in dehydrogenation catalysts with oxidized catalytic species. Many studies have been reported chromium-catalyzed PDH, and it is believed that isolated or low-nuclearity Cr clusters are the active catalysts for CrO_x on both Al_2O_3 and SiO_2 for dehydrogenation[4,7−9] and polymerization.[10−15] Copéret's group demonstrated that Cr^{3+} surface sites were significantly more active than Cr^{2+} sites through heterolytic C−H bond activation as the rate-determining step.[7] There are clearly large effects of both the support oxide and chromium oxide nuclearity.

Single-site catalysts for PDH are particularly interesting as both commercial systems (e.g., Cr and Ga) and as systems to understand the fundamental organometallic reaction mechanisms operative in this catalytic system. Over the past few years, we and others have studied PDH catalysis with a variety of ions[16−19] and found that the overall catalytic rate of PDH by single-site heterogeneous catalysts is primarily governed by one of two basic rate-determining steps: heterolytic cleavage of C−H bond or β-hydride elimination of metal alkyl intermediates.[7,19,20] The heterolytic cleavage of C−H bonds appears to be rate-determining for the transition-metal catalysts Co and

Received: April 30, 2018
Accepted: August 30, 2018
Published: September 13, 2018

DOI: 10.1021/acsomega.8b00862
ACS Omega 2018, 3, 11117−11127

Fe, whereas the β-hydride elimination is rate-determining for main-group ions like Zn and Ga. In addition to the overall rate, the catalytic selectivity of single-site catalysts for C−H activation over C−C bond cleavage appears to be higher for many nanoparticle catalysts. Previous work has shown that while isolated Co[21,22] and Fe[23] sites supported on SiO_2 showed high propene selectivity during PDH under differential conditions, where background thermal cracking is low, the rates are relatively slow compared with Cr-based catalysts. In a more recent study with Y and Sc single-site catalysts and in computational study, we found that the M−O bond strength was a more important descriptor for dehydrogenation rates than the overall Lewis acidity.[24] We reasoned that the catalyst-support oxide bond strength would be more tunable than the rate-determining β-hydride elimination of Zn and Ga catalysts, so we chose to focus on tuning the Lewis acidity of the support for cobalt-based PDH catalysts. For this study, we chose to prepare Zr sites on SiO_2 as a test of this hypothesis that the rate of PDH could be increased while maintaining (or improving) PDH selectivity.

Bulk ZrO_2 has been proved to be a good support for chromium-based dehydrogenation catalysts.[25−32] De Rossi et al. reported that higher dehydrogenation activity was observed over ZrO_2 compared with SiO_2 as a catalyst support for chromium-catalyzed PDH.[33−36] However, the low surface area of ZrO_2 (<100 m^2/g)[28,34,35] resulted in lower overall activity than on Al_2O_3. For the purpose of fundamental study in this work, there are a low number of hydroxyl groups on ZrO_2, likely of many different types that strongly depend on dehydration conditions (cf. Al_2O_3).[37] For this reason, we chose to modify silica with zirconium sites to generate a more well-defined material. For silica-supported catalysts, the ligand can be viewed as ≡SiO−, though distributions of ring sizes and hydroxyl types are also well known.[38−40] Replacing Si with a highly oxophilic metal species, for example Zr, will lead to ≡ZrO− which would be expected to be a weaker electron donating group than ≡SiO−. Such an effect was demonstrated during studies of metal−metal charge-transfer features by the Frei group (cross refs) that showed a decrease of the crystal field splitting energy in tetrahedral Zr−O−Co^{2+} sites versus Si−O−Co^{2+} because of the electrophilicity of the Zr. Consequently, the M−O (M is the isolated catalyst species) bond of ≡ZrO−M species should be weaker than ≡SiO−M. Zirconium sites were grafted on silica (Zr/SiO_2) using $Zr(O^tBu)_4$ as a convenient starting material. Previously, the grafting of Zr though organometallic synthesis have been reported using various precursor compounds[41−49] including $Zr(CH_2CMe_3)_4$,[50] $[(ArO)Zr(CH_2{}^tBu)_3]$,[43] and $Zr(NMe_2)_4$.[51] However, exploration of zirconium and other metals as anchoring sites in well-defined single-site catalysts is relatively unexplored. Zr promotion has been observed for Fischer−Tropsch catalysis[52−54] and Zr on silica is a Lewis acid catalyst for converting glucose to 5-HMF (hydroxymethylfurfural) through isomerization of glucose to fructose.[31,55]

Herein, we report the promotion effect of zirconium addition to the Co/SiO_2 catalysts for nonoxidative dehydrogenation of propane. The change in chemical properties of both Co/SiO_2 and $Co−Zr/SiO_2$ were examined by multiple characterization techniques, including under reaction conditions. Last, the effect of Zr loading to the catalytic activity of $Co−Zr/SiO_2$ and the implications for catalyst dynamic behavior is discussed.

2. EXPERIMENTAL SECTION

2.1. Material and Methods. All manipulations of air-sensitive materials were performed with rigorous exclusion of O_2 and moisture in oven-dried Schlenk-type glassware on a dual manifold Schlenk line and in N_2-filled atmospheres glovebox with a high capacity recirculator (<1 ppm O_2) unless otherwise noted. Solvents were sparged with N_2, dried using activated alumina columns, transferred into the glovebox, and stored over 4 Å molecular sieves prior to use. Unless specified, all chemicals and other solvents were purchased and used as received from Sigma-Aldrich and Strem Chemicals. Elemental analysis (% Co, Zr) was conducted by Galbraith Laboratories, Inc. (Knoxville, TN). Brunauer−Emmett−Teller (BET) surface area and Barrett−Joyner−Halenda (BJH) pore size distribution of the samples were obtained using an accelerated surface area and porosimetry system (ASAP2020) from Micromeritics. The sample was first placed in a sample tube and held under vacuum below 5 μmHg for 30 min. The sample tube was then degassed by increasing the sample tube temperature to 130 °C for 12 h to clean the catalyst surface. After degassing, the sample tube was transferred to the analysis port where nitrogen was physiosorbed at liquid nitrogen temperature. The adsorption isotherms were collected while increasing the pressure of the tube until it reached to nitrogen saturation pressure. BET surface area was calculated on the basis of the adsorption branch of the isotherm, and the BJH pore size distribution was obtained from desorption profile of the isotherm. Transmission electron microscopy (TEM) characterization was performed by using a JEOL JEM2100F microscope equipped with a field emission gun operated at 200 keV. The solid samples were prepared by depositing a diluted sample solution (2.6-Zr/SiO_2, Co/SiO_2, and Co-2.6-Zr/SiO_2 suspended in isopropyl alcohol reagent) on a sample holder (carbon-coated copper grid) and characterized without further treatment. The energy dispersive X-ray spectroscopy (EDX) data were collected on an Oxford Instrument X-Max 80 mm^2 Silicon Drift Detector (SDD) for EDX. The scanning TEM (STEM) experiment was carried out using a FEI Talos microscope operated at 200 kV. Diffuse reflectance infrared fourier transform spectroscopy (DRIFTS) spectra were obtained using a Thermo Scientific Nicolet iS50 FT-IR spectrometer. The sample was packed inside a Praying Mantis reaction cell and sealed with a dome-shaped metal compartment including two ZnSe windows. The reaction chamber was first flushed for 30 min with He to optimize signal intensity. A sample spectrum was acquired by using a MCT/A detector at liquid nitrogen temperature where dried KBr was used as a background. DRUV−vis spectra of the samples were collected by a UV−vis−NIR spectrophotometer—Shimadzu UV-3600 Plus using a PMT (photomultiplier tube) detector. The catalyst was placed on a sample holder under atmosphere condition and the beam was aligned at the center of the sample. The sample spectrum was collected at a medium scan speed with a slit width of 3 nm in the region of 200−800 nm. To have a stable baseline, polytetrafluoroethylene was used as a background. All of the spectra shown in here were transferred to Kubelka−Munk functions. Samples were treated with 3% H_2/Ar using 30 mL/min of flow rate with increasing temperature from RT to 600 °C to obtain temperature programmed reduction (TPR) profiles. The reaction was conducted inside a quartz reactor which was centered in a heated furnace. A thermocouple was inserted into the quartz

DOI: 10.1021/acsomega.8b00862
ACS Omega 2018, 3, 11117−11127

reactor to measure the actual temperature during heating. A ramp rate of 10 °C/min was used. The effluent stream of the reactor was connected to a thermal conductivity detector (TCD) to monitor hydrogen consumption due to the sample. Prior to the experiment, the 3% H_2/Ar gas was first introduced to the reactor continuously to obtain a stable TCD signal. Continuous wave (CW) X-band (9.48 GHz) electron paramagnetic resonance (EPR) experiments were carried out with a Bruker ELEXSYS II E500 EPR spectrometer (Bruker Biospin, Rheinstetten, Germany), equipped with a TE_{102} rectangular EPR resonator (Bruker ER 4102ST). A helium gas-flow cryostat (ICE Oxford, UK) and an intelligent temperature controller (ITC503, Oxford Instruments, UK) were used for measurements at cryogenic temperatures (T = 6 K). Data processing was done using Xepr (Bruker BioSpin, Rheinstetten) and MATLAB 7.11.2 (the MathWorks, Inc., Natick) environment.

2.2. Catalyst Preparation. $Zr(O^tBu)_4$ (2.24 g, 5.7 mmol) was mixed with 2.36 mL anhydrous hexanes to prepare a 4.6 mL stock solution (1.2 M) in a 50 mL round-bottom flask in a N_2 glovebox. The $Zr(O^tBu)_4$ hexanes solution was added dropwise onto 4.6 g silica (dried at 200 °C under vacuum below 5 mTorr) by incipient wetness impregnation. The resulting solid was dried at room temperature under N_2 protection and then was transferred onto the Schlenk line without exposure to air. The material was heated to 100 °C for 20 min under flowing nitrogen, and then the treatment temperature was increased to 200 °C and maintained at 200 °C under vacuum for 1 h, and then the solid was cooled down to room temperature. All synthetic operations were performed under air-free conditions up to this point. After exposure of the resulting material to air at room temperature, 4.92 g of the final product 2.6-Zr/SiO_2 was obtained. Then, the same synthesis method was applied to synthesize 1.3-Zr/SiO_2 (molar ratio of ≡SiOH/Zr = 1:0.5) and 0.26-Zr/SiO_2 (≡SiOH/Zr = 1:0.1).

For Co−Zr/SiO_2 catalysts, strong electrostatic adsorption (SEA)[56] was applied as the synthetic method for preparing low and high loading isolated Co^{2+} on SiO_2 and Zr/SiO_2: 2 g of SiO_2 (Davisil 646, 35−60 mesh, 300 m^2/g and 1.1 cm^3/g, Aldrich) or Zr/SiO_2 were suspended in approximately 20 mL of deionized (DI) water. The pH of the solution was adjusted to 11 by using concentrated ammonium hydroxide (28.0−30.0% NH_3 basis, Aldrich). In a separate flask, 0.3 g of $Co(NH_3)_6Cl_3$ was dissolved in 10 mL of DI water, and the pH was adjusted to 11 with NH_4OH. The basic Co^{3+} solution was rapidly added to the silica and stirred for 10 min at room temperature. The solid was settled for 5 min and the solution decanted. The resulting wet powder was vacuum filtered and rinsed with DI water several times. Then, the solid was dried in air at 125 °C for 2 h. Subsequently, the catalyst was calcined at 550 °C for 3 h with ramping (5 °C/min). Total cobalt loading for Co/SiO_2 by elemental analysis were 1.5 wt %. Total cobalt and zirconium loadings for Co−Zr/SiO_2 by elemental analysis were 1.5 and 6.0 wt %, respectively.

2.3. X-ray Absorption Near Edge Structure (XANES) and Extended X-ray Absorption Fine Structure (EXAFS) Measurements. Co K-edge (7709.0 eV) X-ray absorption spectroscopy (XAS) was measured in transmission mode conducted on the bending magnet beamline of the Materials Research Collaborative Access Team (MRCAT, 10-BM) at the Advanced Photon Source (APS) at Argonne National Laboratory. Ionization chambers were optimized for the maximum current with linear response (ca. 10^{10} photons detected per second) using 20% He in N_2 (15% absorption) in the incident X-ray detector and 25% Ar in N_2 (70% absorption) in the 175 transmission X-ray detector. The energy was calibrated with a cobalt foil (7709.0 eV). Third, the X-ray detector was placed in the beam path beyond the transmission detector to allow acquisition of a reference spectrum concurrent with each sample measurement. The catalyst was pressed as a 4 mm self-supporting wafer and placed in a stainless steel holder. The data were collected for as-prepared, under reaction conditions at 550 °C (3.5% propane in argon), and cooled down to ambient temperature after reaction but without exposure to air. Further XAS data analysis and fitting was processed by using WINXAS 3.2 software. The Co coordination environments were achieved by fitting of EXAFS data in R-space to the first nearest neighbor shell after a Fourier transform (k^2-weighted).

2.4. Catalytic Activity Testing. Catalyst performance testing was conducted in a vertical, quartz tube reactor. Gas flow was controlled using mass flow controllers, and product distribution was determined via online gas chromatography (J&W Scientific) equipped with a 50 m GS-Alumina capillary column and a flame-ionization detector to which H_2 (99.999%, Airgas USA) and air (<2 ppm H_2O, Airgas) were also supplied. In a typical run, approximately 0.5 g of accurately weighed catalyst was supported on quartz wool with an internal thermocouple placed at the top of the catalyst bed. Initially, the catalyst was purged with He (99.999%, Airgas USA) that had been further purified with an oxygen trap at 40 mL/min at room temperature. The temperature was then increased to the reaction temperature of 550 °C and was allowed to stabilize for 2 h before introduction of reactant gases. For PDH, the reaction mixture comprised 3.0% propane in Ar at 20 mL/min.

3. RESULTS AND DISCUSSION

3.1. Synthesis of Zr/SiO_2, Co/SiO_2 and Co−Zr/SiO_2. Zirconium-modified silica was prepared via protonation of $Zr(O^tBu)_4$ by silica hydroxyls at room temperature followed by heating to 200 °C to condense any remaining hydroxyls and thermally cleave *tert*-butoxide groups. A similar synthesis of ZrO_2 thin films by atomic layer deposition (ALD) surface chemistry has been reported by Kukli's group.[57] In our material, we utilized a solution version of an initial nucleation for an ALD reaction by dosing our precursor in solution but with the correct volume to fully saturate the SiO_2 support mesoporous with $Zr(O^tBu)_4$ solution. An equimolar ratio of $Zr(O^tBu)_4$ to isolated hydroxyls (≡SiOH/Zr = 1:1) was used on the basis of the reported OH density after drying at 200 °C (2.5 OH/nm^{-2}).[58] The resulting infrared spectrum and transmission electron micrographs support the uniformity of Zr sites and lack of large crystals of ZrO_x and are discussed more fully below. Our approach is also similar to the one used by Wilson et al.[31,55] to prepare layers of overcoated zirconia on silica by multiple cycles of solution treatment of $Zr(O^iPr)_4$ in anhydrous organic solvent followed by hydrolysis treatment with H_2O. Single-site cobalt 2+ was then grafted onto the low-zirconium density Zr/SiO_2 via SEA using $Co(NH_3)_6Cl_3$ concentrated ammonium hydroxide, where positively charged $Co(NH_3)_6^{3+}$ form cation−anion pairs[56] with the deprotonated surface silica hydroxyls to form an orangish material. When it is heated in air to 300 °C, the Co reduced to Co^{2+} and the color of the material upon air exposure is pink.

3.2. Surface Area, Pore Size and Particle Size. The BET surface area and BJH pore size distribution were acquired

DOI: 10.1021/acsomega.8b00862
ACS Omega 2018, 3, 11117−11127

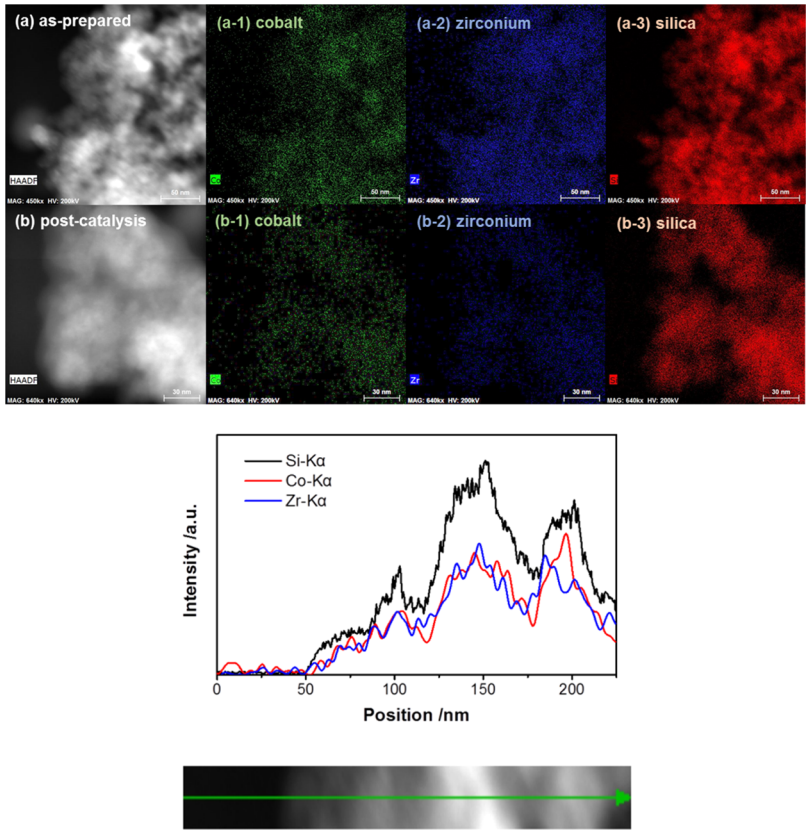

Figure 1. STEM (top) images of (a) as-prepared and (b) post-catalysis Co−Zr/SiO_2 samples and (bottom) the corresponding EDS line scan measured along the as prepared Co−Zr/SiO_2.

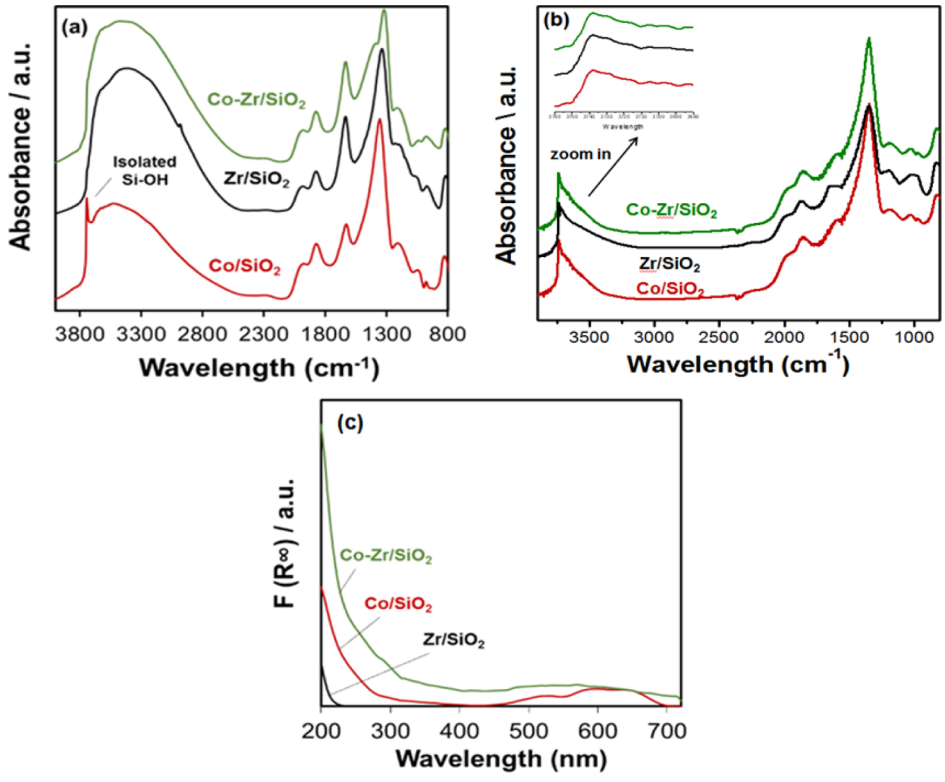

Figure 2. DRIFTS and DRUV−vis spectra of (a) Zr/SiO_2, Co/SiO_2, and Co−Zr/SiO_2 in air, (b) Zr/SiO_2, Co/SiO_2, and Co−Zr/SiO_2 dehydration at 550 °C, and (c) Zr/SiO_2, Co/SiO_2, and Co−Zr/SiO_2 in air.

DOI: 10.1021/acsomega.8b00862
ACS Omega 2018, 3, 11117−11127

for the bare SiO_2, zirconium-modified SiO_2 (Zr/SiO_2), Co/SiO_2 and $Co-Zr/SiO_2$ (plot shown Figure S1). The surface area of commercial SiO_2 is unchanged by the grafting of Zr to make Zr/SiO_2 (324 m^2/g vs 323 m^2/g). Thus, the $Zr(O^tBu)_4$ precursor reacts without producing pore blockage or pore constriction. However, the grafting conditions employed for Co addition resulted method resulted in a loss of surface area of ~50 and ~30 m^2/g for Co/SiO_2 and $Co-Zr/SiO_2$, respectively. This was found to be due to the basic conditions employed during SEA grafting (pH 11), confirmed by a control experiment that omitted cobalt from the synthetic protocol. Despite the small reduction of surface area upon cobalt grafting, the surface areas and pore size distributions are similar and within 300 ± 30 m^2/g (±10%) range.

Conventional TEM (Figure S2) and high-angle annular dark-field–STEM were also utilized to characterize the dispersion and configuration of Co and Zr species on the SiO_2 support for both as-prepared and post-catalysis $Co-Zr/SiO_2$ samples shown in Figure 1a,b. Highly dispersed Co and Zr are observed on the SiO_2 support with similar *Z*-contrast and no aggregation was found post-catalysis, nor carbon nanotubes or other coke deposits. The STEM–EDX elemental mapping result shown in Figure 1 shows that the images of Co, Zr, and Si are completely laid on each other, suggesting that Co sites could be bonded to the Zr or Si sites. The corresponding EDX line scan measured along the sample indicates that there is a relative uniform distribution of Co and Zr atomic sites along with the SiO_2 support.

3.3. DRIFTS and DRUV–Vis Spectroscopy. Comparison of DRIFTS (Figure 2a) shows that in contrast to Co/SiO_2, the zirconium-modified Zr/SiO_2 and $Co-Zr/SiO_2$ do not have isolated OH peaks on the surface by the absence of the peak at 3780 cm^{-1}. A small amount of *tert*-butanol may have remained coordinated during the synthesis of Zr/SiO_2; however, the aqueous cobalt grafting step removes it, as expected, and no C–H ligands are observed to remain on the pre-catalysis $Co-Zr/SiO_2$ catalyst. DRIFTS (Figure 2b) shows that after dehydration at 550 °C, the isolated OH peak appears on the Zr/SiO_2 and $Co-Zr/SiO_2$ surface at 3738 cm^{-1} which is same as Co/SiO_2. No features were resolved that could be ascribed to Zr–OH features on the as-prepared or materials dehydrated at 550 °C.

Visible inspection of Co/SiO_2 and $Co-Zr/SiO_2$ powders post-synthesis shows a striking difference in color, with the Co/SiO_2 displaying a vivid and characteristic "cobalt blue" while the $Co-Zr/SiO_2$ material has a pinkish hue due to water saturation. More careful inspection of the materials using DRUV–vis spectroscopy shows the familiar peaks of the ligand field absorption for isolated tetrahedral Co(II) of the monometallic Co/SiO_2 samples are shown in red in Figure 2c. The UV–vis spectrum exhibits three absorption peaks (530, 595, and 635 nm), which can be explicitly referred to the $^4A_2(F)/^4T_1(P)$ transition of Co(II) ions in tetrahedral geometry.[59,60] The blue shift of the spectrum is similar to that reported for $Co-Zr/SiO_2$ prepared via a different grafting procedure. Additionally, a sharp increase in absorption band in the UV region at 200 nm was observed. This is assigned to a low-energy charge transfer between the oxygen ligands and central Co(II) ion in tetrahedral symmetry. The $Co-Zr/SiO_2$ spectrum in green in Figure 2c shows significantly higher absorption compared with Co/SiO_2 and a small peak at ~300 nm. The increase in intensity is likely attributed to a different geometry of the cobalt environment (tetrahedral to octahedral) which was further confirmed by EXAFS analysis (vide infra). In contrast, CoO nanoparticles display a large, broad peak from 400 to 600 nm,[61,62] again consistent that both of the Co sites are well-dispersed. Zr^{4+} cannot be examined due to weak absorption at $\lambda > 200$ nm.[63,64] The results from DRUV–vis analysis clearly show that the electronic and chemical structure between the as-prepared Co/SiO_2 and $Co-Zr/SiO_2$ are fairly different. However, the familiar pink of $Co(OH_2)_6^{2+}$ ions on the $Co-Zr/SiO_2$ catalyst disappears upon heating, replaced by the characteristic blue of tetrahedral Co^{2+}, which is discussed further below.

EPR is potentially a more sensitive technique for identifying CoO_x clusters than DRIFTS, STEM, or XAS (vide infra). A selected set of EPR spectra recorded under identical experimental conditions at 6 K are shown in Figure 3. The

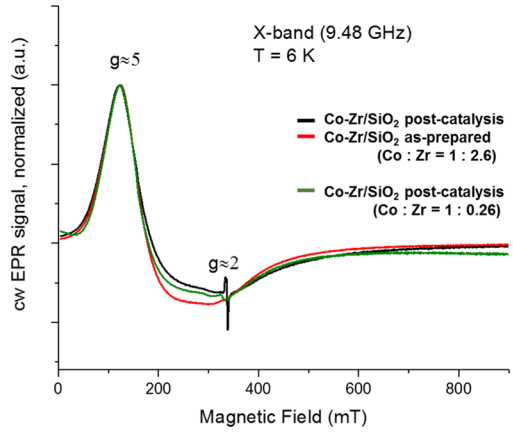

Figure 3. CW X-band EPR spectra obtained from various powder sample of Co/SiO_2 recorded at 6 K.

EPR signals of the three samples are essentially identical. The only difference is in the intensity of the signal, which is due to the concentration of the Co ions in the sample. The main signal is observed at $g_{eff} \approx 5$ together with a broad signal around $g \approx 2$. A substantially narrower signal close to the free electron *g*-value of 2.0023 was observed in $Co-Zr/SiO_2$ post-catalysis. This latter signal is too narrow to be attributed to the cobalt. Most likely this signal is due to trace amounts of radicals/defects often found in powders. These impurities may also be the result of Zr reduction under reaction conditions; however, it is not clear at this time.[65] Our materials have a low coverage of Zr on the silica and absence of large particles of ZrO_2 (vide supra), and isolated Zr^{3+} sites on silica would not be expected to be stable to atmospheric oxygen and moisture. Previous studies have focused on bulk and doped ZrO_2 EPR, rather than submonolayer coverages as in these materials, and we do not have evidence for reduction of Zr in our materials. Our analysis of the possible cobalt EPR-active species is as follows: we have confirmed that the cobalt in our samples is Co(II) via XAS analysis and Co(III) complexes should be EPR-silent under our experimental conditions. While Co(IV) has a low-spin state $S = 1/2$ and gives distinct EPR spectra around $g \approx 2$, this type of signals was not observed in our experiment.[66] On the basis of the findings by Britt and co-workers,[66] the EPR signals observed here belong to Co(II) high spin state ($S = 3/2$), probably in tetrahedral symmetry or axially distorted tetrahedral symmetry,[67] very similar to our previously reported Co/SiO_2 catalysts.[21] Four-coordinated square planar Co(II) complexes as well as square planar

DOI: 10.1021/acsomega.8b00862
ACS Omega 2018, 3, 11117–11127

Co(II) complexes with one or two axial ligands usually demonstrate low-spin state (S = 1/2) and give EPR signals different from those observed here.[68−6971] However, as an alternative explanation, according to Peters and co-workers,[67] it could also be a dimer or multimer of Co(II); as stated by Britt and co-workers:[66] "The feature at $g_{eff} \approx 5$ is reminiscent of EPR spectra measured for many Co(II)-containing compounds, including Co_3O_4, $Co_3(PO_4)_2$." However, no appreciable amounts of Co(III) were detected via XAS, as would be necessary for Co_3O_4 or cobalt phosphate in these materials. Thus EPR was able to demonstrate the absence of CoO but not other potential clusters with different oxidation states. However, bulk XAS analysis was able to exclude the presence of substantial amounts of Co^{3+} and thus the presence of Co_3O_4 clusters, too.

3.4. XANES and EXAFS. In situ XANES and EXAFS spectra of Co/SiO_2 and $Co-Zr/SiO_2$ samples for three different conditions were collected: (1) as-prepared, (2) in situ during dehydrogenation of propane at 550 °C, and (3) post-catalysis at room temperature without exposure to air. Figure 4 shows the XANES spectra of the samples collected under these conditions. The pre-edge energy of Co in all six cases including both Co/SiO_2 and $Co-Zr/SiO_2$ were found to be 7.7092 keV which is consistent with the reported Co^{2+} reference compounds. This evidently indicates that the oxidation state of cobalt of Co/SiO_2 and $Co-Zr/SiO_2$ catalyst remains as +2 during PDH at 550 °C. Consistent with this observation, no consumption of hydrogen was detected from RT to 600 °C during a TPR experiment.

Though the cobalt oxidation of state does *not* change upon heating, the coordination number does change for $Co-Zr/SiO_2$ upon heating, consistent with the color changes and other previously discussed observations. Figure 5 compares the Co

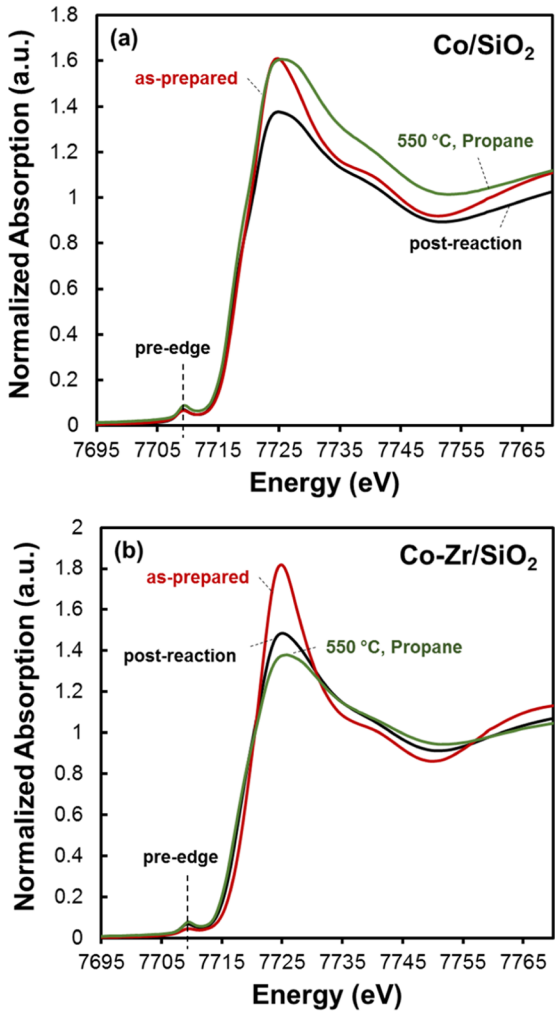

Figure 4. Co K-edge XANES spectra of (a) Co/SiO_2 and (b) $Co-Zr/SiO_2$ samples (1) as-prepared, (2) dehydrogenation reaction condition at 550 °C, and (3) cooled down to RT after catalysis.

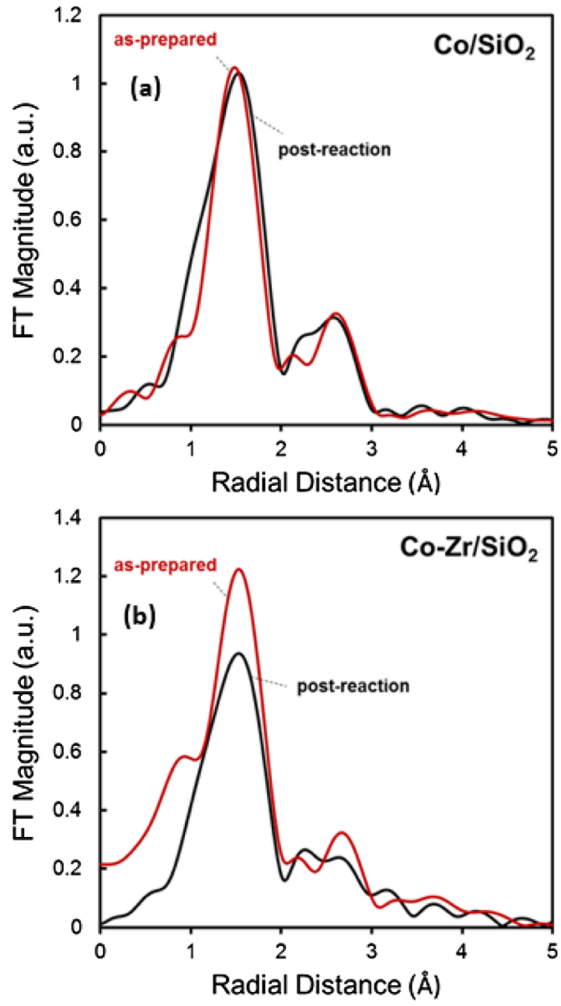

Figure 5. Co K-edge EXAFS spectra of (a) Co/SiO_2 and (b) $Co-Zr/SiO_2$ samples (1) as-prepared and (2) cooled down to RT after catalysis.

K-edge EXAFS spectra between Co/SiO_2 and $Co-Zr/SiO_2$. The first shell peak intensity decreased upon heating as-prepared $Co-Zr/SiO_2$ and fitting of the first shell Co−O peak in EXAFS spectra resulted in coordination number of 6 for as-prepared $Co-Zr/SiO_2$ that decreases to less than 4 on average upon heating (Table 1).

Heating $Co-Zr/SiO_2$ dissociates water with increasing temperate and under reaction conditions (550 °C), the coordination number cobalt drops down to 4.1. Notably, no change in average coordination number was observed for Co/SiO_2. Addition of water on the post-reaction catalyst at RT changes the color of $Co-Zr/SiO_2$ sample back to pink (octahedral) within about half an hour, showing that the cobalt

DOI: 10.1021/acsomega.8b00862
ACS Omega 2018, 3, 11117−11127

Table 1. XANES Pre-Edge Energies and EXAFS Fitting Data of Co/SiO_2 and $Co–Zr/SiO_2$

sample	pre-edge energy (keV)	oxidation state	CN	R (Å)	σ^2	E_0 (eV)	S_0^2
Co/SiO_2 as-prepared	7.7092	+2	3.7 (±0.5)	1.98 (±0.01)	0.005	−8.5 (±2.0)	0.81
Co/SiO_2 post-reaction	7.7092	+2	4.0 (±0.8)	1.97 (±0.02)	0.008	−2.0 (±3.2)	0.82
$Co–Zr/SiO_2$ as-prepared	7.7092	+2	5.7 (±0.7)	2.05 (±0.01)	0.009	−7.9 (±1.7)	0.88
$Co–Zr/SiO_2$ post-reaction	7.7092	+2	4.1 (±0.6)	1.99 (±0.02)	0.009	−4.0 (±2.2)	0.86

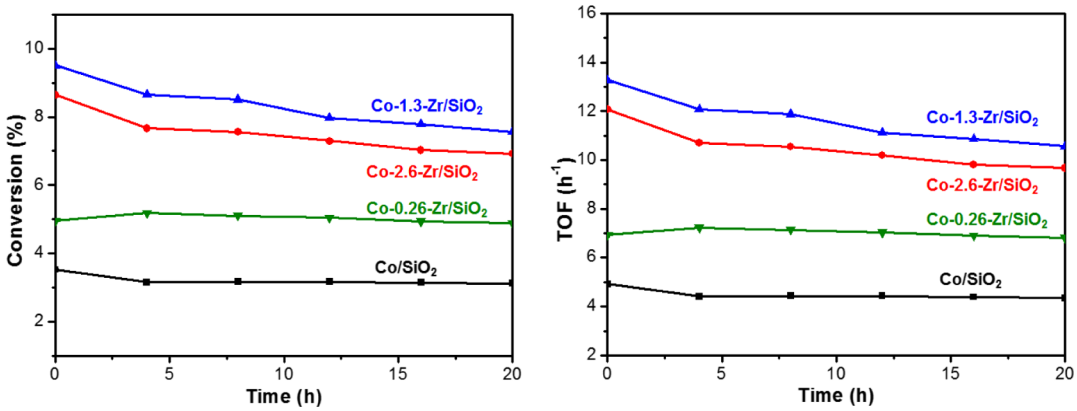

Figure 6. Comparison of PDH reactivity performed at 550 °C, propane (3% in Ar) flow rate is 20 mL/min, using Co/SiO_2 and $Co–Zr/SiO_2$ with increasing Zr loading (numbers indicate molar ratio of Co to Zr).

surface hydration is reversible and that Co sites remain isolated after PDH catalysis.

The fitted Co–O bond distances are different but not significantly so. The Co–O distances in $Co–Zr/SiO_2$ (as-prepared = 2.05 ± 0.01 Å, post-reaction = 1.99 ± 0.02 Å) was found to be slightly longer than that of Co/SiO_2 (as-prepared = 1.98 ± 0.01 Å, post-reaction = 1.97 ± 0.02 Å). However, these distances are notably longer than the reported Co–O bond of Co_3O_4 nanoparticles supported on SiO_2 reduced at 553 K of 1.91 Å.[72] Thus, while the average Co–O bond distances when supported on SiO_2 and Zr/SiO_2 are not significantly different, the fact that the cobalt of $Co–Zr/SiO_2$ is hydrated/dehydrated readily is also consistent with a weaker cobalt–support interaction than Co/SiO_2, which does not hydrate, and is consistent with the red shift in the UV–vis spectrum of $Co–Zr/SiO_2$.

3.5. Catalytic PDH. The catalytic activity of $Co–Zr/SiO_2$ and Co/SiO_2 were compared under similar reaction conditions (at 550 °C, propane flow rate is 20 mL/min), with conversion levels controlled to below 10% in remain in the kinetically-controlled regime. The turnover frequency (TOF) value obtained over $Co–Zr/SiO_2$ catalyst was found to be 10.0 h^{-1} (±10%) at 550 °C, which is three times faster than that of Co/SiO_2. A control experiment under the same reaction conditions using the bare Zr/SiO_2 support shows negligible catalytic activity for PDH and thus there is no contribution from Zr/SiO_2 to the catalytic activity of the $Co–Zr/SiO_2$ catalyst. This is in contrast to reports of ZrO_2 and doped $MZrO_2$ (M = La etc.) materials, where coordinatively unsaturated Z_{CUS} are proposed as active participants.[32] We do not have evidence that single-site zirconium on silica has similar catalytic behavior under these conditions. Also of note, O^{2-} ion mobility varies widely with doping levels in doped MO_x materials.[73−75] In addition to having a higher PDH rate than Co/SiO_2, $Co–Zr/SiO_2$ also shows higher propene selectivity at 550 °C of ∼97% versus the Co/SiO_2 catalyst of 93%. It should be noted that in most heterogeneous catalyst systems, the selectivity decreases as the conversion increases. However, in this case, both selectivity *and* rate for $Co–Zr/SiO_2$ are higher than the zirconium-free catalyst. The catalysts are stable on-stream for at least 20 h and negligible coke formation (>99% carbon balance during the run). Finally, the reversible hydration of the cobalt led us to test whether long-term storage under ambient conditions would lead to different catalyst behavior. We found that after storage in air for 1 month, samples of $Co–Zr/SiO_2$ catalysts have no detectible change in catalytic behavior when tested. These results, together with the STEM images of the post-catalysis $Co–Zr/SiO_2$ catalysts (Figure 1) provide clear evidence that no nanoparticles are forming under reaction conditions, in contrast to cobalt on silica catalysts reported by Coperet.[22]

The different cobalt hydration behavior and catalytic function were obtained for $Co–Zr/SiO_2$ containing excess zirconium sites with ratio of zirconium to cobalt of ca. 2.6:1; however, we lowered the ratio of Zr to Co for two reasons: (1) to see if there was a preference for cobalt to reside near a zirconium site on the surface of the silica and (2) to see if there is differing activity with lower density of zirconia. Thus, we found that at a 1:1.3 ratio of Co and Zr the PDH rate and selectivity were unchanged from $Co–Zr/SiO_2$ (2.6:1 ratio) within error. Further lowering of the amount of zirconium to substoichiometric 1:0.26 resulted in an observed PDH rate that is approximately the weighted average of the Co/SiO_2 and $Co–Zr/SiO_2$ rates, also consistent with cobalt sites being directly promoted by the Zr (Figure 6). The selectivity of the PDH was found to be ca. 97% for all $Co–Zr/SiO_2$ species (Figure 7). It is reasonable to expect that a labile octahedral Co^{2+} ion would be able to traverse the surface prior to dehydration based upon our previous observation of the dispersal of CoO clusters, so we infer that these results to show some thermodynamic preference for Co–O–Zr≡ linkages, though further study is clearly needed and in progress.

Our proposed structures for the distribution of cobalt sites in the varying $Co–Zr/SiO_2$ catalysts are summarized in Figure 8. The surface Co^{2+} comprises two types of sites, Co atoms adjacent to the ≡Zr–OH and Co sites that are not adjacent to

DOI: 10.1021/acsomega.8b00862
ACS Omega 2018, 3, 11117−11127

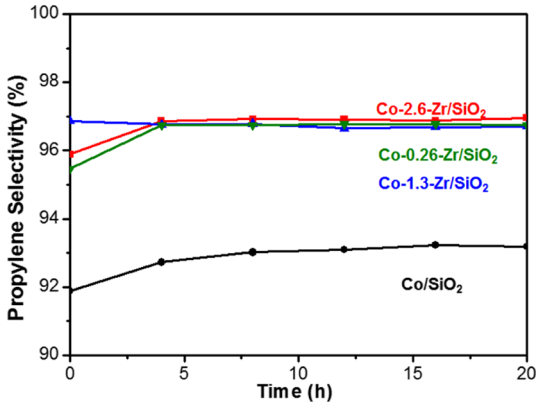

Figure 7. Comparison of PDH selectivity performed at 550 °C, propane (3% in Ar) flow rate is 20 mL/min, using Co/SiO_2 and $Co-Zr/SiO_2$ with increasing Zr loading (numbers indicate molar ratio of Co to Zr).

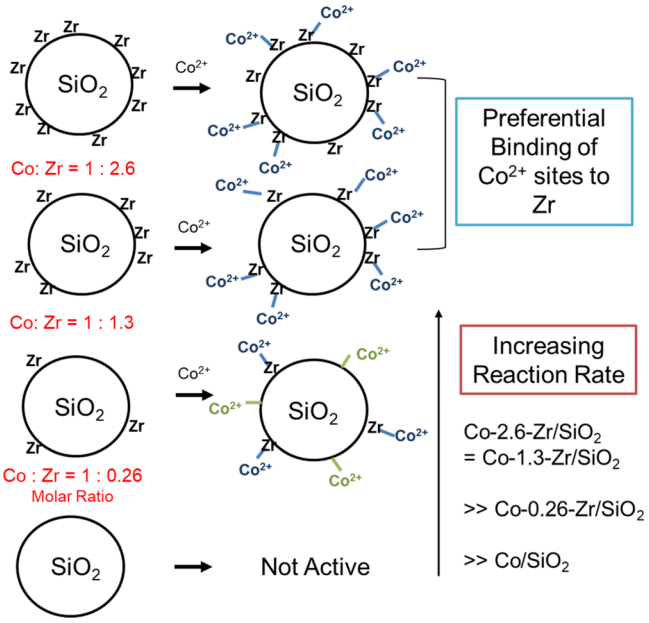

Figure 8. Cartoon representation of the ratio of Zr−Co in catalyst materials and $Co-Zr/SiO_2$ catalyst site distribution. The Co−X lines (SiO_2 or Zr) represent Co−O−X bonds.

the ≡Zr−OH (neglecting siloxane ring size effects). When excess or stoichiometric zirconium sites are present, octahedral cobalt 2+ ions are preferentially associated with them. They are hydrolytically labile and hydrate under air but dehydrate to tetrahedral Co^{2+} under reaction conditions. Because of the highly dispersed zirconium, it is also possible to assume that Zr might deposit randomly on the catalyst surface. However, in this case, the substoichiometric zirconium loadings would not be expected to be populated by adjacent cobalt sites as a weighted average, as inferred from the TOF of the working catalysts. Furthermore, the observed weighted average TOF is also not consistent with more than one cobalt associating with a zirconium site. Thus, we hypothesize that this system has a thermodynamic preference for a cobalt to be adjacent to a surface zirconium, if one exists, and that these sites are both faster for PDH as well as more selective.

In addition to the location of Co relative to Zr on the SiO_2 surface, some discussion of the electronic impact of the electrophilic Zr is needed. Our $Co-Zr/SiO_2$ catalyst shows similar UV−vis shifts as previous work by Macnaughtan, Soo, and Frei[60] due to electron-withdrawing Zr decreasing the π donation of O ligand into transition-metal Co and a widening of the d-orbital splitting. This lowers the Co−O bond strength and results in a larger splitting energy between e and t_2 orbitals of $Co-Zr/SiO_2$ than Co/SiO_2 (Figure 9). Altering the π-donating ability of a ligand, a common strategy for tuning rate and selectivity in homogeneous catalysis, is less understood for single-site ionic catalysts such as these. The increase in rate due to the electron-withdrawing effects of Zr is consistent with our previous calculations,[40] that shows that decreasing the catalyst−oxygen bond strength leads to an increase in PDH rate. Although the impact on PDH rate in this specific case was a modest increase, the increase in catalytic selectivity to propene (ca. 92−97%) was significant. This observation shows that relatively small perturbations in catalyst−support bond strengths can result in significant changes in not only C−H heterolytic cleavage, the rate-determining step of dehydrogenation but also the catalytic selectivity of the reaction. The origin of the change in selectivity is not understood at this time and is the subject of ongoing work.

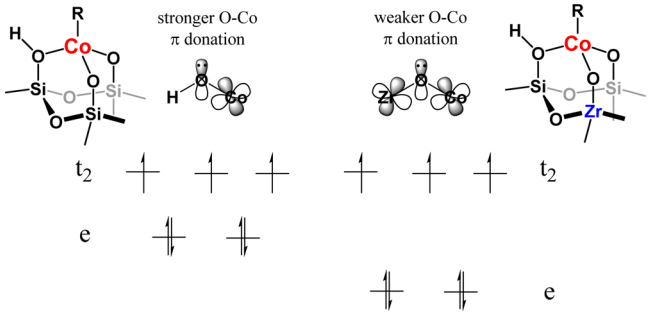

Figure 9. Diagram of the Co(II) splitting energy between (left) Co/SiO_2 and (right) $Co-Zr/SiO_2$. Adapted from ref 60.

4. CONCLUSION

Higher turnover frequencies were observed for the Zr-promoted cobalt catalysts with significant increase in propane conversion and propene selectivity compared with the Co/SiO_2 catalyst. The relationship between Zr loading and catalyst selectivity is consistent with the formation of enhanced active sites at the interface between the Co metal and the Zr promoter atom. As Zr loading increases, the active sites adjacent to the promoter increases. Ultimately, the fraction of active sites that are promoted approaches unity, suggesting that this occurs near a Zr/Co atomic ratio of 1, and no further improvements to the product selectivity result from higher Zr loading. This suggests the Lewis acidity of the promoter is the relevant descriptor for metal oxide promotion effects. The improved dehydrogenation activity was attributed to the ease of heterolytic cleavage of the C−H bond over a weaker Co−O bond of ≡Zr−O−Co. The positive effects of having weaker M−O bond for facial heterolytic cleavage leads to a promising strategy for rational catalyst design.

DOI: 10.1021/acsomega.8b00862
ACS Omega 2018, 3, 11117−11127

■ ASSOCIATED CONTENT

Supporting Information

The Supporting Information is available free of charge on the ACS Publications website at DOI: 10.1021/acsomega.8b00862.

BET surface areas and BJH pore size distributions, TEM images and analysis, data processing and analysis of EXAFS measurements, and dehydrogenation with Co/ZrO_2 results (PDF)

■ AUTHOR INFORMATION

Corresponding Author

*E-mail: ahock@iit.edu (A.S.H.).

ORCID

Jens Niklas: 0000-0002-6462-2680
Oleg G. Poluektov: 0000-0003-3067-9272
Massimiliano Delferro: 0000-0002-4443-165X
Adam S. Hock: 0000-0003-1440-1473

Present Addresses

∥Korea Institute of Science and Technology (H.S.).
⊥Phillips 66 (B.H.).

Notes

The authors declare no competing financial interest.

■ ACKNOWLEDGMENTS

This research was supported by the U.S. Department of Energy (DOE), Office of Basic Energy Sciences, Division of Chemical Sciences, Biosciences and Geosciences under contract DE-AC02-06CH11357. Use of the Advanced Photon Source (APS) and the Center for Nanoscale Materials (CNM) at Argonne National Laboratory was supported by the U.S. Department of Energy, Office of Science, and Office of Basic Energy Sciences, under contract DE-AC02-06CH11357. MRCAT operations are supported by the Department of Energy and the MRCAT member institutions.

■ REFERENCES

(1) Sattler, J. J. H. B.; Ruiz-Martinez, J.; Santillan-Jimenez, E.; Weckhuysen, B. M. Catalytic Dehydrogenation of Light Alkanes on Metals and Metal Oxides. *Chem. Rev.* **2014**, *114*, 10613−10653.

(2) Bariås, O. A.; Holmen, A.; Blekkan, E. A. Propane Dehydrogenation over Supported Pt and Pt-Sn Catalysts: Catalyst Preparation, Characterization, and Activity Measurements. *J. Catal.* **1996**, *158*, 1−12.

(3) Stagg, S. M.; Querini, C. A.; Alvarez, W. E.; Resasco, D. E. Isobutane Dehydrogenation on Pt-Sn/SiO_2 Catalysts: Effect of Preparation Variables and Regeneration Treatments. *J. Catal.* **1997**, *168*, 75−94.

(4) Hakuli, A.; Kytökivi, A.; Krause, A. O. I. Dehydrogenation of i-butane on CrOx/Al_2O_3 catalysts prepared by ALE and impregnation techniques. *Appl. Catal., A* **2000**, *190*, 219−232.

(5) Michorczyk, P.; Pietrzyk, P.; Ogonowski, J. Preparation and characterization of SBA-1-supported chromium oxide catalysts for CO2 assisted dehydrogenation of propane. *Microporous Mesoporous Mater.* **2012**, *161*, 56−66.

(6) Feng, J.; Zhang, M.; Yang, Y. Dehydrogenation of Propane on Pt or PtSn Catalysts with Al_2O_3 or SBA-15 Support. *Chin. J. Chem. Eng.* **2014**, *22*, 1232−1236.

(7) Conley, M. P.; Delley, M. F.; Núñez-Zarur, F.; Comas-Vives, A.; Copéret, C. Heterolytic Activation of C-H Bonds on Cr^{III}-O Surface Sites Is a Key Step in Catalytic Polymerization of Ethylene and Dehydrogenation of Propane. *Inorg. Chem.* **2015**, *54*, 5065−5078.

(8) Delley, M. F.; Silaghi, M.-C.; Nuñez-Zarur, F.; Kovtunov, K. V.; Salnikov, O. G.; Estes, D. P.; Koptyug, I. V.; Comas-Vives, A.; Copéret, C. X-H Bond Activation on Cr(III),O Sites (X = R, H): Key Steps in Dehydrogenation and Hydrogenation Processes. *Organometallics* **2017**, *36*, 234−244.

(9) Coperet, C. C−H Bond Activation and Organometallic Intermediates on Isolated Metal Centers on Oxide Surfaces. *Chem. Rev.* **2010**, *110*, 656−680.

(10) Ajjou, J. A. N.; Scott, S. L.; Paquet, V. Synthesis and Characterization of Silica-Stabilized Chromium(IV) Alkylidene Complexes. *J. Am. Chem. Soc.* **1998**, *120*, 415−416.

(11) Ajjou, J. A. N.; Scott, S. L. A Kinetic Study of Ethylene and 1-Hexene Homo- and Copolymerization Catalyzed by a Silica-Supported Cr(IV) Complex: Evidence for Propagation by a Migratory Insertion Mechanism. *J. Am. Chem. Soc.* **2000**, *122*, 8968−8976.

(12) Brown, C.; Krzystek, J.; Achey, R.; Lita, A.; Fu, R.; Meulenberg, R. W.; Polinski, M.; Peek, N.; Wang, Y.; van de Burgt, L. J.; Profeta, S.; Stiegman, A. E.; Scott, S. L. Mechanism of Initiation in the Phillips Ethylene Polymerization Catalyst: Redox Processes Leading to the Active Site. *ACS Catal.* **2015**, *5*, 5574−5583.

(13) Brown, C.; Lita, A.; Tao, Y.; Peek, N.; Crosswhite, M.; Mileham, M.; Krzystek, J.; Achey, R.; Fu, R.; Bindra, J. K.; Polinski, M.; Wang, Y.; van de Burgt, L. J.; Jeffcoat, D.; Profeta, S.; Stiegman, A. E.; Scott, S. L. Mechanism of Initiation in the Phillips Ethylene Polymerization Catalyst: Ethylene Activation by Cr(II) and the Structure of the Resulting Active Site. *ACS Catal.* **2017**, *7*, 7442−7455.

(14) Fong, A.; Peters, B.; Scott, S. L. One-Electron-Redox Activation of the Reduced Phillips Polymerization Catalyst, via Alkylchromium-(IV) Homolysis: A Computational Assessment. *ACS Catal.* **2016**, *6*, 6073−6085.

(15) Fong, A.; Yuan, Y.; Ivry, S. L.; Scott, S. L.; Peters, B. Computational Kinetic Discrimination of Ethylene Polymerization Mechanisms for the Phillips (Cr/SiO_2) Catalyst. *ACS Catal.* **2015**, *5*, 3360−3374.

(16) Thomas, J. M.; Raja, R.; Lewis, D. W. Single-site Heterogeneous Catalysts. *Angew. Chem., Int. Ed.* **2005**, *44*, 6456−6482.

(17) Nozaki, C.; Lugmair, C. G.; Bell, A. T.; Tilley, T. D. Synthesis, Characterization, and Catalytic Performance of Single-Site Iron(III) Centers on the Surface of SBA-15 Silica. *J. Am. Chem. Soc.* **2002**, *124*, 13194−13203.

(18) Yun, D.; Baek, J.; Choi, Y.; Kim, W.; Lee, H. J.; Yi, J. Promotional Effect of Ni on a CrO_x Catalyst Supported on Silica in the Oxidative Dehydrogenation of Propane with CO_2. *ChemCatChem* **2012**, *4*, 1952−1959.

(19) Schweitzer, N. M.; Hu, B.; Das, U.; Kim, H.; Greeley, J.; Curtiss, L. A.; Stair, P. C.; Miller, J. T.; Hock, A. S. Propylene Hydrogenation and Propane Dehydrogenation by a Single-Site Zn^{2+} on Silica Catalyst. *ACS Catal.* **2014**, *4*, 1091−1098.

(20) Chen, K.; Bell, A. T.; Iglesia, E. Kinetics and Mechanism of Oxidative Dehydrogenation of Propane on Vanadium, Molybdenum, and Tungsten Oxides. *J. Phys. Chem. B* **2000**, *104*, 1292−1299.

(21) Hu, B.; Getsoian, A.; Schweitzer, N. M.; Das, U.; Kim, H.; Niklas, J.; Poluektov, O.; Curtiss, L. A.; Stair, P. C.; Miller, J. T.; Hock, A. S. Selective propane dehydrogenation with single-site Co^{II} on SiO_2 by a non-redox mechanism. *J. Catal.* **2015**, *322*, 24−37.

(22) Estes, D. P.; Siddiqi, G.; Allouche, F.; Kovtunov, K. V.; Safonova, O. V.; Trigub, A. L.; Koptyug, I. V.; Copéret, C. C-H Activation on Co,O Sites: Isolated Surface Sites versus Molecular Analogs. *J. Am. Chem. Soc.* **2016**, *138*, 14987−14997.

(23) Hu, B.; Schweitzer, N. M.; Zhang, G.; Kraft, S. J.; Childers, D. J.; Lanci, M. P.; Miller, J. T.; Hock, A. S. Isolated Fe^{II} on Silica As a Selective Propane Dehydrogenation Catalyst. *ACS Catal.* **2015**, *5*, 3494−3503.

(24) Camacho-Bunquin, J.; Aich, P.; Ferrandon, M.; Getsoian, A.; Das, U.; Dogan, F.; Curtiss, L. A.; Miller, J. T.; Marshall, C. L.; Hock, A. S.; Stair, P. C. Single-site Zinc on Silica Catalysts for Propylene Hydrogenation and Propane Dehydrogenation: Synthesis and

DOI: 10.1021/acsomega.8b00862
ACS Omega 2018, 3, 11117−11127

Reactivity Evaluation Using an Integrated Atomic Layer Deposition-catalysis Instrument. *J. Catal.* **2017**, *345*, 170−182.
(25) Brückner, A.; Radnik, J.; Hoang, D.-L.; Lieske, H. In Situ Investigation of Active Sites in Zirconia-supported Chromium Oxide Catalysts During the Aromatization of n-octane. *Catal. Lett.* **1999**, *60*, 183−189.
(26) Cimino, A.; Cordischi, D.; De Rossi, S.; Ferraris, G.; Gazzoli, D.; Indovina, V.; Minelli, G.; Occhiuzzi, M.; Valigi, M. Studies on chromia/zirconia catalysts I. Preparation and characterization of the system. *J. Catal.* **1991**, *127*, 744−760.
(27) Khodakov, A.; Yang, J.; Su, S.; Iglesia, E.; Bell, A. Structure and properties of vanadium oxide-zirconia catalysts for propane oxidative dehydrogenation. *J. Catal.* **1998**, *177*, 343−351.
(28) Cutrufello, M. G.; De Rossi, S.; Ferino, I.; Monaci, R.; Rombi, E.; Solinas, V. Preparation, characterisation and activity of chromia−zirconia catalysts for propane dehydrogenation. *Thermochim. Acta* **2005**, *434*, 62−68.
(29) Xu, B.; Zheng, B.; Hua, W.; Yue, Y.; Gao, Z. Support effect in dehydrogenation of propane in the presence of CO_2 over supported gallium oxide catalysts. *J. Catal.* **2006**, *239*, 470−477.
(30) Jiménez-López, A.; Rodríguez-Castellón, E.; Maireles-Torres, P.; Díaz, L.; Mérida-Robles, J. Chromium Oxide Supported on Zirconium- and Lanthanum-doped Mesoporous Silica for Oxidative Dehydrogenation of Propane. *Appl. Catal., A* **2001**, *218*, 295−306.
(31) Osatiashtiani, A.; Lee, A. F.; Granollers, M.; Brown, D. R.; Olivi, L.; Morales, G.; Melero, J. A.; Wilson, K. Hydrothermally Stable, Conformal, Sulfated Zirconia Monolayer Catalysts for Glucose Conversion to 5-HMF. *ACS Catal.* **2015**, *5*, 4345−4352.
(32) Otroshchenko, T. P.; Rodemerck, U.; Linke, D.; Kondratenko, E. V. Synergy effect between Zr and Cr active sites in binary $CrZrO_x$ or supported CrO_x /$LaZrO_x$: Consequences for catalyst activity, selectivity and durability in non-oxidative propane dehydrogenation. *J. Catal.* **2017**, *356*, 197−205.
(33) De Rossi, S.; Ferraris, G.; Fremiotti, S.; Garrone, E.; Ghiotti, G.; Campa, M. C.; Indovina, V. Propane Dehydrogenation on Chromia/Silica and Chromia/Alumina Catalysts. *J. Catal.* **1994**, *148*, 36−46.
(34) De Rossi, S.; Ferraris, G.; Fremiotti, S.; Cimino, A.; Indovina, V. Propane Dehydrogenation on Chromia/Zirconia Catalysts. *Appl. Catal., A* **1992**, *81*, 113−132.
(35) De Rossi, S.; Ferraris, G.; Fremiotti, S.; Indovina, V.; Cimino, A. Isobutane Dehydrogenation on Chromia/Zirconia Catalysts. *Appl. Catal., A* **1993**, *106*, 125−141.
(36) De Rossi, S.; Pia Casaletto, M.; Ferraris, G.; Cimino, A.; Minelli, G. Chromia/Zirconia Catalysts with Cr Content Exceeding the Monolayer. A comparison with Chromia/Alumina and Chromia/Silica for Isobutane Dehydrogenation. *Appl. Catal., A* **1998**, *167*, 257−270.
(37) Wischert, R.; Laurent, P.; Copéret, C.; Delbecq, F.; Sautet, P. γ-Alumina: The Essential and Unexpected Role of Water for the Structure, Stability, and Reactivity of "Defect" Sites. *J. Am. Chem. Soc.* **2012**, *134*, 14430−14449.
(38) Zhuravlev, L. T. Concentration of Hydroxyl Groups on the Surface of Amorphous Silicas. *Langmuir* **1987**, *3*, 316−318.
(39) Zhuravlev, L. T. The Surface Chemistry of Amorphous Silica. Zhuravlev model. *Colloids Surf., A* **2000**, *173*, 1−38.
(40) Das, U.; Zhang, G.; Hu, B.; Hock, A. S.; Redfern, P. C.; Miller, J. T.; Curtiss, L. A. Effect of Siloxane Ring Strain and Cation Charge Density on the Formation of Coordinately Unsaturated Metal Sites on Silica: Insights from Density Functional Theory (DFT) Studies. *ACS Catal.* **2015**, *5*, 7177−7185.
(41) Copéret, C.; Comas-Vives, A.; Conley, M. P.; Estes, D. P.; Fedorov, A.; Mougel, V.; Nagae, H.; Núñez-Zarur, F.; Zhizhko, P. A. Surface Organometallic and Coordination Chemistry toward Single-Site Heterogeneous Catalysts: Strategies, Methods, Structures, and Activities. *Chem. Rev.* **2016**, *116*, 323−421.
(42) El Eter, M.; Hamzaoui, B.; Abou-Hamad, E.; Pelletier, J. D. A.; Basset, J.-M. Well-defined Azazirconacyclopropane Complexes Supported on Silica Structurally Determined by 2D NMR Comparative Elucidation. *Chem. Commun.* **2013**, *49*, 4616−4618.
(43) Guillemot, G.; Thieuleux, C.; Copéret, C.; Soulivong, D.; Spitzmesser, S.; Basset, J.-M. Modifying the Reactivity in the Homologation of Propane by Introducing Aryloxide Ligands on a Silica Supported Zirconium Alkyl System. *Dalton Trans.* **2007**, 4589−4593.
(44) Calucci, L.; Forte, C.; Pampaloni, G.; Pinzino, C.; Renili, F. Chemical Implantation of Group 4 Cations on Silica via Cyclopentadienyl- and N,N-dialkylcarbamato Derivatives. *Inorg. Chim. Acta* **2010**, *363*, 33−40.
(45) Jezequel, M.; Dufaud, V.; Ruiz-Garcia, M. J.; Carrillo-Hermosilla, F.; Neugebauer, U.; Niccolai, G. P.; Lefebvre, F.; Bayard, F.; Corker, J.; Fiddy, S.; et al. Supported Metallocene Catalysts by Surface Organometallic Chemistry. Synthesis, Characterization, and Reactivity in Ethylene Polymerization of Oxide-Supported Mono- and Biscyclopentadienyl Zirconium Alkyl Complexes: Establishment of Structure/Reactivity Relationships. *J. Am. Chem. Soc.* **2001**, *123*, 3520−3540.
(46) Popoff, N.; Gauvin, R. M.; De Mallmann, A.; Taoufik, M. On the Fate of Silica-Supported Half-Metallocene Cations: Elucidating a Catalyst's Deactivation Pathways. *Organometallics* **2012**, *31*, 4763−4768.
(47) Millot, N.; Soignier, S.; Santini, C. C.; Baudouin, A.; Basset, J.-M. Synthesis, Characterization, and Activity in Ethylene Polymerization of Silica Supported Cationic Cyclopentadienyl Zirconium Complexes. *J. Am. Chem. Soc.* **2006**, *128*, 9361−9370.
(48) Salinier, V.; Niccolai, G. P.; Dufaud, V.; Basset, J.-M. Silica-Supported Zirconium Complexes and their Polyoligosilsesquioxane Analogues in the Transesterification of Acrylates: Part 2. Activity, Recycling and Regeneration. *Adv. Synth. Catal.* **2009**, *351*, 2168−2177.
(49) Thornburg, N. E.; Thompson, A. B.; Notestein, J. M. Periodic Trends in Highly Dispersed Groups IV and V Supported Metal Oxide Catalysts for Alkene Epoxidation with H_2O_2. *ACS Catal.* **2015**, *5*, 5077−5088.
(50) Alladin, T.; Beaudoin, M. C.; Scott, S. L. Thermolysis of Silica-Supported Bis(neopentyl) Complexes of Titanium and Zirconium. *Inorg. Chim. Acta* **2003**, *345*, 292−298.
(51) Popoff, N.; Espinas, J.; Pelletier, J.; Macqueron, B.; Szeto, K. C.; Boyron, O.; Boisson, C.; Del Rosal, I.; Maron, L.; De Mallmann, A.; et al. Small Changes Have Consequences: Lessons from Tetrabenzyltitanium and -zirconium Surface Organometallic Chemistry. *Chem.—Eur. J.* **2013**, *19*, 964−973.
(52) Feller, A.; Claeys, M.; van Steen, E. Cobalt Cluster Effects in Zirconium Promoted Co/SiO_2 Fischer−Tropsch Catalysts. *J. Catal.* **1999**, *185*, 120−130.
(53) Ali, S.; Chen, B.; Goodwin, J. G. Zr Promotion of Co/SiO_2 for Fischer-Tropsch Synthesis. *J. Catal.* **1995**, *157*, 35−41.
(54) Zhang, H.; Ma, H.; Zhang, H.; Ying, W.; Fang, D. Effects of Zr and K Promoters on Precipitated Iron-Based Catalysts for Fischer-Tropsch Synthesis. *Catal. Lett.* **2011**, *142*, 131−137.
(55) Morales, G.; Osatiashtiani, A.; Hernández, B.; Iglesias, J.; Melero, J. A.; Paniagua, M.; Brown, D. R.; Granollers, M.; Lee, A. F.; Wilson, K. Conformal Sulfated Zirconia Monolayer Catalysts for the One-pot Synthesis of Ethyl Levulinate from Glucose. *Chem. Commun.* **2014**, *50*, 11742−11745.
(56) Dsouza, L.; Jiao, L.; Regalbuto, J.; Miller, J.; Kropf, A. Preparation of Silica- and Carbon-Supported Cobalt by Electrostatic Adsorption of Co(III) Hexaammines. *J. Catal.* **2007**, *248*, 165−174.
(57) Kukli, K.; Ritala, M.; Leskelä, M. Low-Temperature Deposition of Zirconium Oxide-Based Nanocrystalline Films by Alternate Supply of $Zr[OC(CH_3)_3]_4$ and H_2O. *Chem. Vap. Deposition* **2000**, *6*, 297−302.
(58) Rascón, F.; Wischert, R.; Copéret, C. Molecular Nature of Support Effects in Single-Site Heterogeneous Catalysts: Silica vs Alumina. *Chem. Sci.* **2011**, *2*, 1449.
(59) Kim, W.; Yuan, G.; McClure, B. A.; Frei, H. Light Induced Carbon Dioxide Reduction by Water at Binuclear $ZrOCo^{II}$ Unit

DOI: 10.1021/acsomega.8b00862
ACS Omega 2018, 3, 11117−11127

Coupled to Ir Oxide Nanocluster Catalyst. *J. Am. Chem. Soc.* **2014**, *136*, 11034−11042.
(60) Macnaughtan, M. L.; Soo, H. S.; Frei, H. Binuclear ZrOCo Metal-to-Metal Charge-Transfer Unit in Mesoporous Silica for Light-Driven CO_2 Reduction to CO and Formate. *J. Phys. Chem. C* **2014**, *118*, 7874−7885.
(61) Di Carlo, G.; Liotta, L. F.; Pantaleo, G.; Venezia, A. M.; Deganello, G. Alumina and Alumina-Baria Supported Cobalt Catalysts for DeNO x : Influence of the Support and Cobalt Content on the Catalytic Performance. *Top. Catal.* **2009**, *52*, 1826−1831.
(62) Lu, A.; Chen, Y.; Zeng, D.; Li, M.; Xie, Q.; Zhang, X.; Peng, D.-L. Shape-related Optical and Catalytic Properties of Wurtzite-type CoO Nanoplates and Nanorods. *Nanotechnology* **2014**, *25*, 035707.
(63) Emeline, A. V.; Kuzmin, G. N.; Basov, L. L.; Serpone, N. Photoactivity and photoselectivity of a dielectric metal-oxide photocatalyst (ZrO_2) probed by the photoinduced reduction of oxygen and oxidation of hydrogen. *J. Photochem. Photobiol., A* **2005**, *174*, 214−221.
(64) Fernández López, E.; Sánchez Escribano, V.; Panizza, M.; Carnasciali, M. M.; Busca, G. Vibrational and Electronic Spectroscopic Properties of Zirconia Powders. *J. Mater. Chem.* **2001**, *11*, 1891−1897.
(65) Gionco, C.; Paganini, M. C.; Giamello, E.; Burgess, R.; Di Valentin, C.; Pacchioni, G. Paramagnetic Defects in Polycrystalline Zirconia: An EPR and DFT Study. *Chem. Mater.* **2013**, *25*, 2243−2253.
(66) McAlpin, J. G.; Surendranath, Y.; Dincă, M.; Stich, T. A.; Stoian, S. A.; Casey, W. H.; Nocera, D. G.; Britt, R. D. EPR Evidence for Co(IV) Species Produced During Water Oxidation at Neutral pH. *J. Am. Chem. Soc.* **2010**, *132*, 6882−6883.
(67) Jenkins, D. M.; Di Bilio, A. J.; Allen, M. J.; Betley, T. A.; Peters, J. C. Elucidation of a Low Spin Cobalt(II) System in a Distorted Tetrahedral Geometry. *J. Am. Chem. Soc.* **2002**, *124*, 15336−15350.
(68) Malatesta, V.; McGarvey, B. R. Single Crystal Electron Spin Resonance Of Low Spin Co(II) And Of Cu(II) Schiff Base Complexes. *Can. J. Chem.* **1975**, *53*, 3791−3800.
(69) Niklas, J.; Mulfort, K. L.; Rakhimov, R. R.; Mardis, K. L.; Tiede, D. M.; Poluektov, O. G. The Hydrogen Catalyst Cobaloxime − a Multifrequency EPR and DFT Study of Cobaloxime's Electronic Structure. *J. Phys. Chem. B* **2012**, *116*, 2943−2957.
(70) McGarvey, B. R. Theory of the Spin Hamiltonian Parameters for Low Spin Cobalt(II) Complexes. *Can. J. Chem.* **1975**, *53*, 2498−2511.
(71) Nishida, Y.; Kida, S. Splitting of d-orbitals in square planar complexes of copper(II), nickel(II) and cobalt(II). *Coord. Chem. Rev.* **1979**, *27*, 275−298.
(72) Ernst, B.; Bensaddik, A.; Hilaire, L.; Chaumette, P.; Kiennemann, A. Study on a Cobalt Silica Catalyst during Reduction and Fischer-Tropsch Reaction: In situ EXAFS Compared to XPS and XRD. *Catal. Today* **1998**, *39*, 329−341.
(73) Gilardi, E.; Gregori, G.; Wang, Y.; Sigle, W.; van Aken, P. A.; Maier, J. Interface Effects on the Ion Transport of Epitaxial $Y_2Zr_2O_7$ Films. *ACS Appl. Mater. Interfaces* **2017**, *9*, 27257−27265.
(74) Levy, M.; Fouletier, J. Influence of Dopant Concentration on the Electronic Conductivity of Nonstoichiometric Yttria-Doped Ceria. *Solid State Ionics* **1984**, *12*, 467−472.
(75) Kimpton, J.; Randle, T. H.; Drennan, J. Investigation of electrical conductivity as a function of dopant-ion radius in the systems $Zr_{0.75}Ce_{0.08}M_{0.17}O_{1.92}$ (M=Nd, Sm, Gd, Dy, Ho, Y, Er, Yb, Sc). *Solid State Ionics* **2002**, *149*, 89−98.

DOI: 10.1021/acsomega.8b00862
ACS Omega 2018, 3, 11117−11127